ACS OMEGA

http://pubs.acs.org/journal/acsodf

Article

Combination of Plasmon-Mediated Photochemistry and Seed-Mediated Methods for Synthesis of Bicomponent Nanocrystals

Hsien-Tai Cheng,‡ Ming-Shiuan Huang,‡ and Su-Wen Hsu*

Cite This: *ACS Omega* 2022, 7, 30622−30631

Read Online

ACCESS | Metrics & More | Article Recommendations | Supporting Information

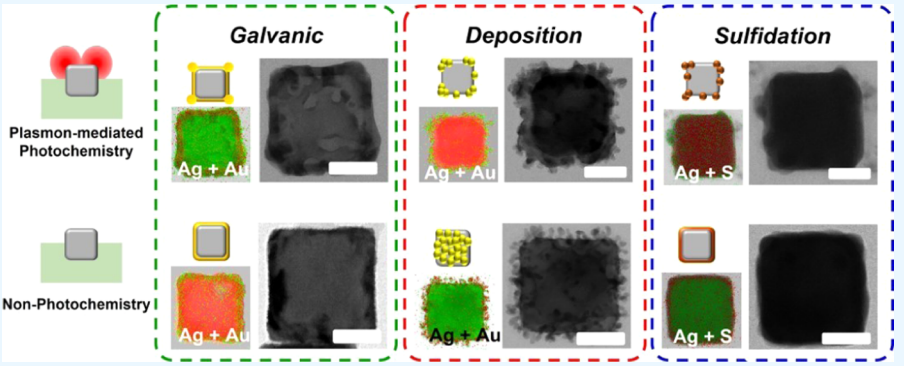

ABSTRACT: Plasmon resonances of metal nanocrystals resulted from free electrons oscillating around nanocrystals, leading to a strong electromagnetic field around them. Because these oscillating electrons possess higher energy than the original ones, also known as hot electrons, these were widely used as photocatalysts for various reactions. Also, the strength and distribution of the electromagnetic field around the nanocrystals strongly depended on their morphology and excited irradiation, which led to the reaction environment around nanocrystals being controllable. Here, we integrated the seed-mediated and plasmon-mediated photochemistry methods for fabricating bimetallic and semiconductor−metal nanocrystals with controllable morphologies and compositions of the nanocrystals, resulting from the highly anisotropic reaction environment around the nanocrystals. The highly anisotropic reaction environment around the template nanocrystal was caused by the distribution of electromagnetic fields around it and its exposure area in the reaction solution. This new synthesis method should enable the fabrication of various multicomponent nanocrystals with desirable functions for potential applications, such as photocatalysts, chemical sensors, biosensors, biomedicines, etc.

1. INTRODUCTION

Photochemistry utilized clean and unlimited sunlight energy for enhancing the various chemical reactions that caused it to attract wide attention in the last few decades. Since the enhancement factor of the photochemical reactions depended on the amount of sunlight energy, efficient light-absorbing materials or absorption structures played an important role in photochemical reactions.[1−10] Due to the excellent light-absorbing properties of plasmonic nanocrystals, such as silver nanocrystals, these nanocrystals had been shown to be useful as "plasmon photocatalysis";[11−18] for example, photodecomposition of methylene blue can be enhanced using plasmonic nanocrystals as catalysts. Plasmonic nanocrystals were also used to trigger or accelerate many other chemical reactions that led to plasmonic nanocrystals with potential applications in photochemistry, such as plasmon-mediated nanomedicine, energy, and catalysis.[19−26] These plasmon-mediated effects can be attributed to the localized electromagnetic field around nanocrystals, excitation of hot electrons, and local heating around nanocrystals.[27−33] These phenomena were caused by the free carriers in metals or heavily doped semiconductor oscillation on their surfaces, also known as localized surface plasmon resonance, LSPR. Despite the various applications of plasmonic nanocrystals, it is difficult to find relevant studies using plasmonic properties to control the formation of multicomponent morphologies and components of nanocrystals.

In addition, the quality of plasmonic properties of nanocrystals strongly depended on the morphology of plasmonic nanostructures, excitation wavelength, excitation polarization, etc., which made it possible to control photochemical reactivity by changing the morphology of plasmonic

Received: July 9, 2022
Accepted: August 5, 2022
Published: August 16, 2022

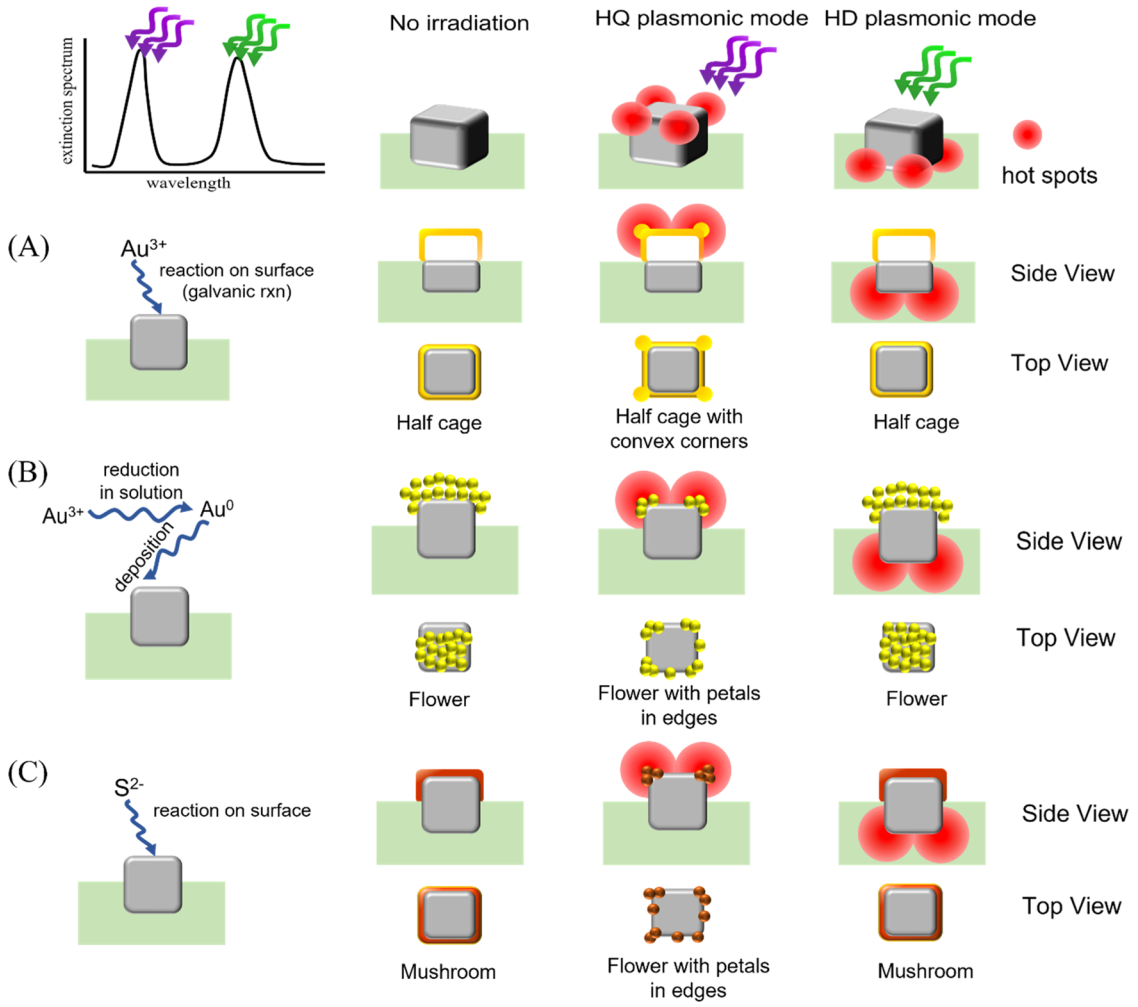

Figure 1. Schematic of the formation of bicomponent nanocrystals by combining "seed"-mediated and "plasmon"-mediated synthetic methods. (A) Half-cage Ag−Au alloy nanocrystals generated by the galvanic replacement reaction of Au^{3+} ions on the surface of AgNCs, (B) flowerlike Ag−Au nanocrystals generated by deposition of Au atoms on the surface of AgNCs, and (C) flowerlike Ag_2S-Ag nanocrystals generated by the reaction of S^{-2} ions on the surface of AgNCs.

nanocrystal.[34−41] Nanocrystals with high anisotropic morphology under light irradiation had stronger electromagnetic fields in the higher-curvature portion of nanocrystals, which led to the generation of higher anisotropic photochemical reactivity around nanocrystals. Theoretically, the anisotropic photochemical reaction environment surrounding nanocrystals can serve as the nanoscale templates (seed) for the fabrication of highly anisotropic and multicomponent nanocrystals. Recently, our group demonstrated that an anisotropic reaction environment can be established around metallic nanocrystals by partial embedding nanocrystals in the polymer (heterogeneous interface). These partial embedding nanocrystals can be used as "seeds" for the fabrication of highly anisotropic bimetallic nanocrystals under redox reactions.[42] The anisotropic reaction environment surrounding nanocrystals under light irradiation may also be used to fabricate multicomponent nanocrystals. Compared with the anisotropic reaction environment created by placing the nanocrystals on a heterogeneous interface, the plasmon-induced anisotropic reaction environment around the nanocrystals was more tunable, which benefited from the high sensitivity of the plasmon-induced electromagnetic field to excitation wavelength and morphology of nanocrystals. The highly sensitive anisotropic reaction environment surrounding nanocrystals should be used as "seeds" for the fabrication of multicomponent nanocrystals with well-controlled compositions and morphologies.

Here, we used the highly anisotropic plasmonic nanocrystals—silver nanocubes (AgNCs)—as "seeds" for the fabrication of bimetallic nanocrystal and metal−semiconductor nanocrystals through plasmon-mediated photochemical reactions. AgNCs were placed on a polymer matrix to build an anisotropic reaction environment induced by a heterogenous interface, and the plasmonic nanocrystal−polymer composite was irradiated with light to generate a "plasmon"-induced anisotropic reaction environment. This "dual" anisotropic reaction environment can be used to control the composition and morphology of bicomponent nanocrystals produced under photochemical reactions (as schematically shown in Figure 1). AgNCs partially embedded in a polystyrene (PS) matrix exhibited two plasmon resonance modes under irradiation: a hybrid dipole (HD) mode at a longer wavelength and a hybrid quadrupole (HQ) mode at a shorter wavelength.

The HD plasmonic mode of AgNC−PS nanocomposites corresponded to the electromagnetic field established at the top corners of AgNC (the part exposed to the PS film); the HQ plasmonic mode of AgNC−PS nanocomposite corre-

https://doi.org/10.1021/acsomega.2c04349
ACS Omega 2022, 7, 30622−30631

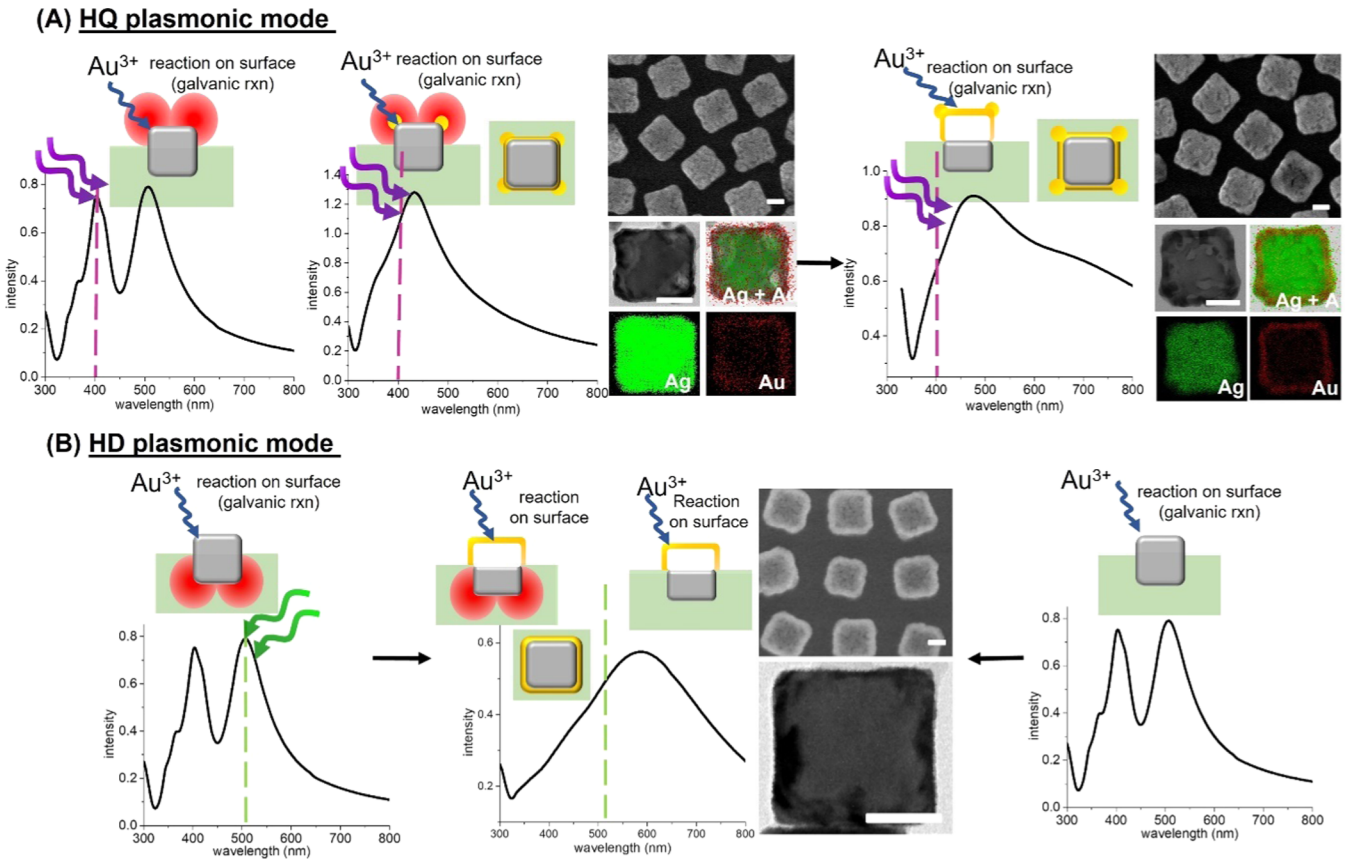

Figure 2. Plasmon-mediated synthesis of bimetallic nanocrystals by the galvanic replacement reaction. (A) Due to the reduction of Au^{3+} ions on the surface of AgNC and the electromagnetic field established at the top corners of AgNC under light irradiation in the HQ mode (purple dashed line), the morphology of nanocrystals was transformed from AgNC to porous AgNC with a convex-corner and then to a convex-corner half-cage structure. (B) Under the same reaction conditions, the final product structure of bimetallic nanocrystals synthesized under light irradiation in the HD mode (green dashed line) was a half-cage nanocrystal, which was similar to that of bimetallic nanocrystals synthesized without irradiation. UV−vis spectra of the nanocomposites were used to examine the plasmonic mode changes of the nanocrystal templates during the reaction. The morphology changes of the bimetallic nanocrystals during the reaction were observed by SEM and TEM images. Scale bar = 50 nm.

sponded to the electromagnetic field established at the bottom corners of AgNC (the part embedded in the PS film) (as schematically shown in Figure 1).[43] In terms of bimetallic nanocrystals, Au−Ag alloy nanocrystals can be fabricated by two different reaction mechanisms: reduction of Au^{3+} ions on the AgNC surface or deposition of Au atoms on the AgNC surface. These two reaction mechanisms can be manipulated by controlling the concentration of the reducing agent in the reaction solution, resulting in half-cage-like nanocrystals and flowerlike nanocrystals.[42] Under the influence of the plasmon-mediated electromagnetic field, the Au^{3+} ions or Au atoms preferentially reacted on the corners of AgNC to generate a half-cage with convex-corner structure and petals located at the edges of the flower, respectively, as schematically shown in Figure 1A,B.

For the formation of Ag_2S−Ag nanocrystals, in the absence of plasmon-mediated electromagnetic field, the precursor of S^{2-} preferentially deposited and reacted uniformly on the surface of AgNCs to generate a mushroom-like structure. However, under the influence of the plasmon-mediated electromagnetic field, the morphology of the Ag_2S−Ag nanocrystal had the structure of petals located at the flower edges, which was caused by the electromagnetic field located at the corners of AgNCs, as schematically shown in Figure 1C.

These results suggested that a combination of plasmon-mediated photochemical reactions and seed-mediated synthetic methods can be utilized to fabricate bicomponent nanocrystals with well-controlled compositions and morphologies, which can be attributed to the anisotropic reaction environment around nanocrystals. This novel synthesis method made it possible to design multicomponent nanocrystals with desired multifunctional properties. These multicomponent nanocrystals possessed excellent optical and electronic properties, which benefited from the "synergetic" coupling effect between different materials. These materials had potential applications in catalysis, sensing, bioimaging, and optoelectronics.

2. RESULTS AND DISCUSSIONS

To study the effect of plasmonic photochemical reaction on the morphology and composition of bicomponent nanocrystal during seed-mediated synthesis, high-quality plasmonic nanocrystals—silver nanocubes (AgNCs), were used as "seeds", which showed strong plasmon-induced electromagnetic field appeared around the highly curved edges and corners of AgNCs. The nonuniform distribution of the electromagnetic fields on the surface of the nanocrystal led to a highly anisotropic reaction environment on the host nanocrystal (seed), which affected the reaction of the guest material on the host nanocrystal. AgNCs were placed on a polystyrene (PS) surface, a heterogeneous interface", which not only enhanced

https://doi.org/10.1021/acsomega.2c04349
ACS Omega 2022, 7, 30622−30631

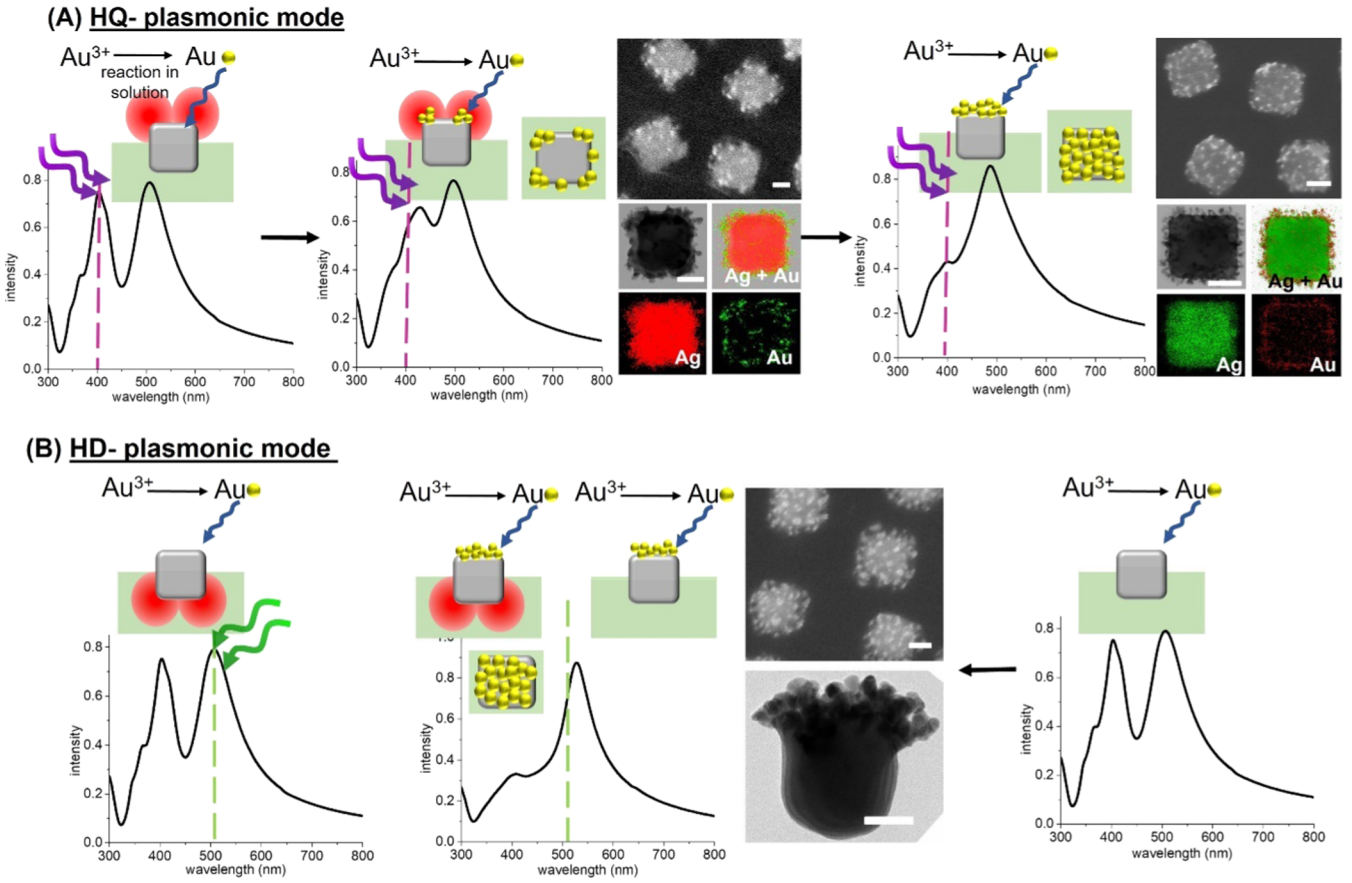

Figure 3. Plasmon-mediated synthesis of bimetallic nanocrystals by deposition of Au atoms. (A) Au^{3+} ions were reduced to Au atoms in the solution and then deposited on the surface of AgNC under light irradiation in the HQ mode (purple dashed line). During the reaction, the morphology of nanocrystals changed from AgNCs to structures with petals located at the edges and corners of the flower. (B) Under the same reaction conditions, the bimetallic nanocrystals were synthesized under light irradiation in the HD mode (green dashed line); the final product of bimetallic nanocrystals was petals uniformly distributed in flowerlike nanocrystals, with the same structure as bimetallic nanocrystals synthesized without irradiation. UV−vis spectra of the nanocomposites were used to examine the plasmonic mode changes of the nanocrystal templates during the reaction. The morphological changes of the bimetallic nanocrystals during the reaction were observed by SEM and TEM images. Scale bar = 50 nm.

the anisotropic reaction environment around AgNC but also overcame the shortcomings of solution-based reactions.[42] To optimize the plasmonic photochemical reaction on AgNCs, the frequency of light irradiation for the photochemical reaction needed to correspond to the frequency of plasmon resonance of the AgNC−PS nanocomposite. The plasmon resonance formed by AgNCs partially embedded in the PS matrix possessed two plasmonic modes: a hybrid dipole (HD) mode at 520 nm and a hybrid quadrupole (HQ) mode at 410 nm. Since the AgNCs were partially embedded in the PS film, the top and bottom corners of AgNCs showed different reactivity for the guest material: the photochemical reaction enhanced the reactivity of the top corners of AgNCs, and PS film suppressed the reactivity of the bottom portion of AgNC due to blocking up the reaction of precursors. This highly anisotropic reaction environment around AgNCs under light irradiation at HQ and HD modes led to the highly anisotropic morphology of bicomponent nanocrystals. Theoretically, plasmon-mediated electromagnetic fields were used to enhance the photochemical reactions to generate highly anisotropic bicomponent nanocrystals, which included all reactions involving "electron conversion".

Here, two different guest materials, gold ion (Au^{3+}) and sulfide ion (S^{2-}), were reacted with host templates (AgNCs) to fabricate bimetallic and metal−semiconductor nanocrystals, respectively. For the fabrication of bimetallic Au−Ag nanocrystal, there were two different reaction mechanisms: (1) Au^{3+} ions reducing on the surface of AgNC; (2) Au^{3+} ions reducing to Au atoms in aqueous solution, and then deposition on the surface of AgNC, as shown in Figure 2A,B, respectively. The reduction reaction of Au^{3+} ions on the AgNC surface and the deposition of Au atoms on the AgNC surface were affected by the plasmon-induced electromagnetic field around AgNC. For AgNC−PS nanocomposites under HQ mode light irradiation, a strong electromagnetic field was generated at the top corner of ANC above the PS matrix, also known as hotspots, Au^{3+} ions preferentially moved to the hotspots, and then formed a galvanic replacement reaction on the surface of AgNC, $3Ag^0 + Au^{3+} \rightarrow Au + 3Ag^+$, which led to the convex-corner of the Au−Ag alloy structure on the corners of the AgNC template, as schematic and scanning electron microscopy (SEM) and transmission electron microscopy (TEM) images show in Figure 2A. The formation of the plasmon-induced electromagnetic field around AgNC is also accompanied by the formation of hot electrons and localized thermal effect that should enhance photochemical reactions and lead to the generation of highly heterogeneous bimetallic nanocrystals.

https://doi.org/10.1021/acsomega.2c04349
ACS Omega 2022, 7, 30622−30631

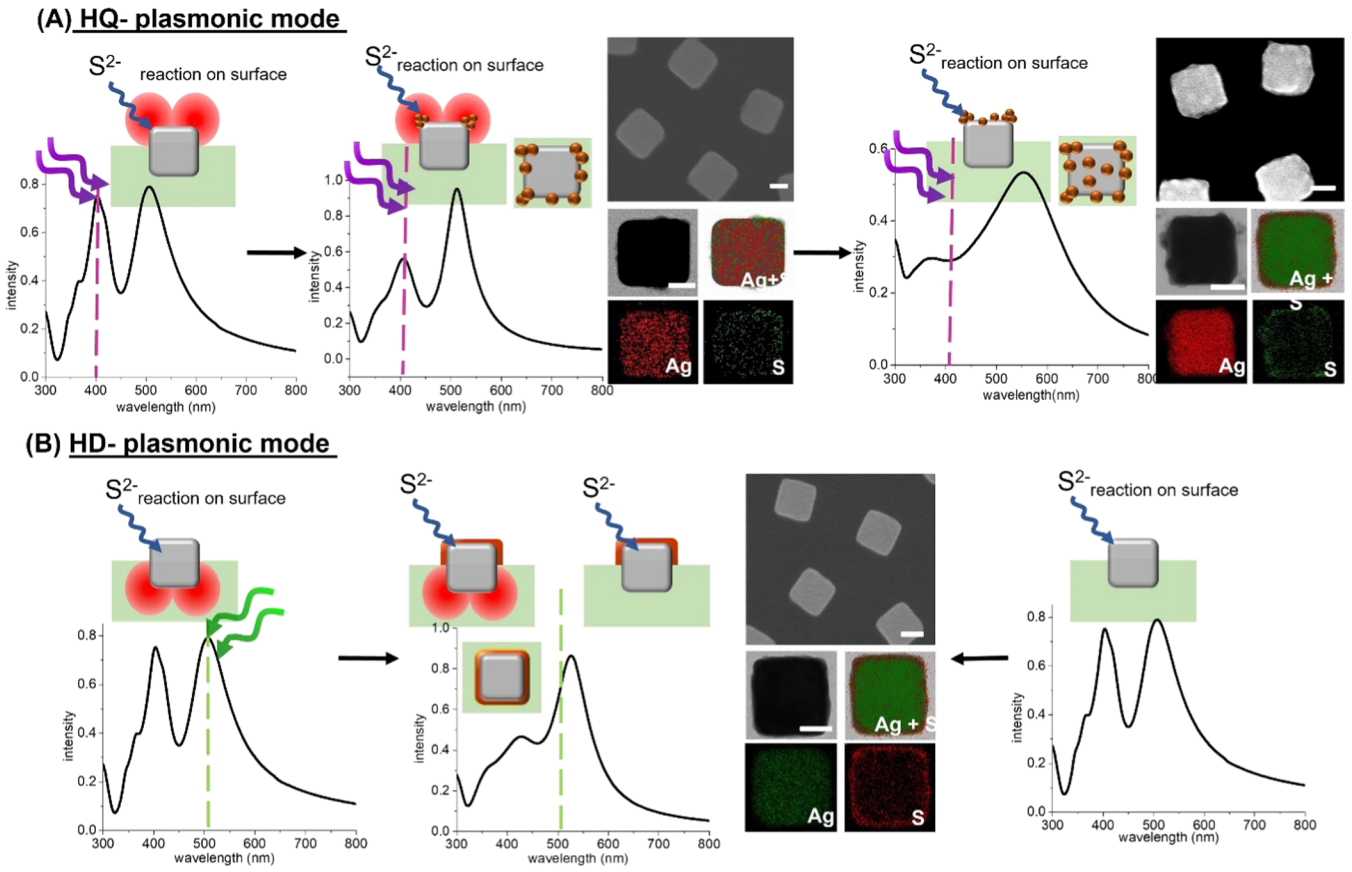

Figure 4. Plasmon-mediated synthesis of metal−semiconductor nanocrystals by the sulfidation reaction on the AgNC surface. (A) Sulfidation reaction preferentially occurred at the top corners of AgNCs, which was consistent with the location of the electromagnetic field on the surface of AgNCs under light irradiation in the HQ plasmonic mode (purple dashed line). The morphology of nanocrystals changed from AgNC to petals located at the edges/corners of the flower structure during the reaction. (B) For the metal−semiconductor nanocrystals synthesized under light irradiation in the HD mode (green dashed line) with the same reaction conditions, the final product of bicomponent nanocrystals was mushroom-like nanocrystals, which was similar to the nanocrystals synthesized without irradiation. UV−vis spectra of the nanocomposites were used to examine the plasmonic mode changes of the nanocrystal templates during the reaction. The morphological changes in the bimetallic nanocrystals during the reaction were observed by SEM and TEM images. Scale bar = 50 nm.

As three Ag atoms were consumed to generate one Au atom during the galvanic replacement reaction, this led to the formation of nanocrystals with empty spaces inside and convex corners (as the TEM image shows in the middle panel of Figure 2A). Galvanic replacement occurred at the top corners of AgNCs, which resulted in the formation of convex-cornered nanocrystals and the diminishing of the HQ mode of the nanocrystals, as shown in the UV−vis spectrum in the middle panel of Figure 2A and Supporting Information Figure S1A. The diminishing of the HQ mode led to the weakening of the electromagnetic field strength around the corners of the AgNCs and the formation of convex-cornered half-cage-like nanocrystals, as shown in the TEM image in the right panel of Figure 2A.

To confirm the effect of plasmon-induced electromagnetic field on the photochemical reaction (the morphology of bimetallic nanocrystals formed by phoyochemical reaction), bimetallic nanocrystals generated by the reduction of Au^{3+} ions on the surface of AgNC under light irradiation at 520 nm (the HD mode of the AgNC−PS nanocomposite corresponded to the bottom angle of the electromagnetic field on AgNC). The morphology of bimetallic nanocrystals showed half-cage-like nanocrystals with sharper corners (as SEM and TEM images show in Figure 2B), which was identical to the morphology of bimetallic nanocrystals produced without light irradiation (evidence of morphology half-cage-like nanocrystal with sharper corners, such as energy-dispersive X-ray (EDX) mapping analysis, can be found in the previous report).[42] This result was due to the fact that galvanic replacement occurred only on the AgNC surface exposed to the reaction solution. Also, the galvanic replacement process took place preferentially on the high-curvature edges and corners of AgNC, which were less protected by ligands. The frequency of irradiation in the HD mode resulted in hotspots on the bottom corners of AgNCs in the PS matrix, and the reduction of Au^{3+} ions on these hotspots was inhibited by the PS matrix. The plasmon resonance of the nanocomposites during the formation of Au−Ag nanocrystals, with and without light irradiation in the HD mode, showed that the HQ and HD modes merged into one plasmon mode and then underwent a red-shift (shown in Figure 2B and Supporting Information Figure S1B).

Another possible reaction mechanism for the fabrication of bimetallic nanocrystals was the reduction of Au^{3+} ions to Au atoms in the solution, which were then deposited on the surface of AgNCs, which can be achieved by increasing the concentration of the reducing agent (poly(vinylpyrrolidone), PVP) in the reaction solution.[42] The deposition of Au atoms

https://doi.org/10.1021/acsomega.2c04349
ACS Omega 2022, 7, 30622−30631

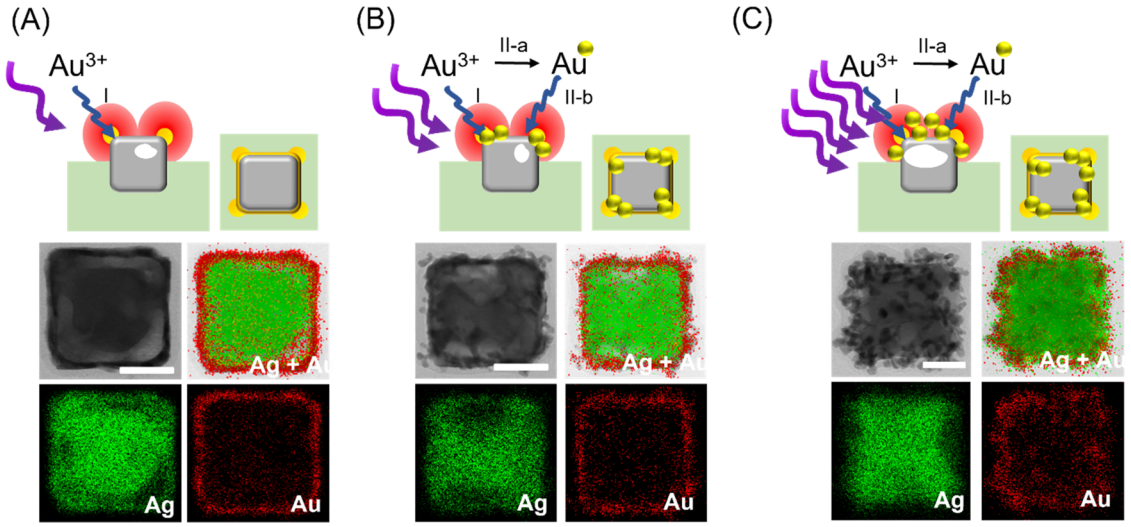

Figure 5. Bimetallic nanocrystals are synthesized by the plasmon-mediated method with different excitation intensities but with the same irradiation frequency. (A) Under the light irradiation of HQ mode frequency, the morphology of bimetallic nanocrystals was a convex-corner half-cage structure generated by the reduction of Au^{3+} ions on the surface of AgNCs. When the light intensity was doubled, the Au^{3+} ions were reduced not only on the AgNC surface but also in the reaction solution, which led to the morphology of bimetallic nanocrystals to be a mixed structure: flowerlike and convex-corner half-cage structure as shown in (B). When the irradiation intensity was increased by a factor of four, the flowerlike structure became more obvious, as shown in (C). Scale bar = 50 nm.

on the surface of AgNC was also affected by the plasmon-induced electromagnetic field, resulting in the attachment of small Au nanocrystals to the top corners of the AgNCs and the generation of a structure in which the petals were located at the edges and corners of a flower, as shown in the middle panel in Figure 3A. During the formation of bimetallic nanocrystals, the HQ plasmonic mode of the nanocomposite at 410 nm red-shifted and merged with the HD plasmonic mode into one plasmonic mode, which also resulted in the weakening of the electromagnetic field and the decrease of the number of hot electrons at the top corners of AgNCs (shown in Figure 3A and Supporting Information Figure S1C). The weakening of the electromagnetic field and the decrease of the number of hot electrons around the AgNC surface led to a more uniform reaction environment (weakening the photocatalytic effect of bimetallic nanocrystal formation), resulting in flowerlike nanocrystals: the petals were uniformly deposited on the AgNC surface, as shown in the right panel in Figure 3A. The bimetallic nanocrystals generated under light irradiation in the HD mode (520 nm) also showed the formation of flowerlike nanocrystals, which was consistent with the morphology of bimetallic nanocrystals in the absence of irradiation, as TEM and SEM images show in Figure 3B (evidence of the morphology of half-cage-like nanocrystals with sharper corners, such as EDX mapping analysis, can be found in the previous report).[42] Also, the change of the nanocomposite plasmonic modes during the reaction also showed a similar trend (as shown in Supporting Information Figure S1D). The shrinking of the size and decrease of the curvature at the bottom part of flowerlike nanocrystals (shown in the TEM image in Figure 3B) were caused by the diffusion of Ag atoms to the top portion of the nanocrystal.[42]

The formation of bimetallic nanocrystals formation with or without external irradiation is mainly obtained by two competing reaction mechanisms, which make the surface of bimetallic nanocrystals crystallize as polycrystalline or alloy rather than single crystalline. Bimetallic nanocrystals with polycrystalline or alloy had been also observed in previous reports.[44,45]

The bimetallic nanocrystals synthesized by the plasmon-mediated method can be also used to generate metal−-semiconductor nanocrystals. Plasmonic AgNCs were used as templates to fabricate Ag_2S-Ag bicomponent nanocrystals using S^{2-} ions as precursors for the sulfidation reaction. The sulfidation reaction on the AgNC surface preferentially occurred at the top corners of AgNC (consistent with the plasmon-induced electromagnetic field established under light irradiation in HD mode), leading to petals located at the edges/corners of the flower structure, as shown in the middle panel in Figure 4A.

The strength of the HQ mode of the nanocomposite weakened during the sulfidation reaction, resulting in a weakening of the electromagnetic field around the AgNCs and reformation of a uniform reaction environment (as shown in Supporting Information Figure S1E). The final morphology of Ag_2S-Ag nanocrystals showed flowerlike nanocrystals with small Ag_2S spots generated on all AgNC surfaces exposed to the reaction solution (shown as SEM and TEM images in the right panel of Figure 4A). When the sulfidation reaction was performed under light irradiation in the HD mode or without light irradiation, the AgNC surface exposed outside the PS matrix had a uniform sulfidation reaction environment, which led to the formation of a uniformly covered Ag_2S shell covered on the exposed portion of AgNC outside the PS matrix, also known as mushroom-like structure (as SEM and TEM images show in Figure 4B and Supporting Information Figure S2).

For the formation of the highly anisotropic bicomponent nanocrystals by integrating seed-mediated and plasmon-mediated photochemical reactions, the frequency of the irradiation light played an important role in controlling the location of the formation of the second component on the template nanocrystal. The irradiation light not only generated an electromagnetic field on the surface of the template nanocrystals but also accelerated the reduction reaction of the second component in the reaction solution. During the

https://doi.org/10.1021/acsomega.2c04349
ACS Omega 2022, 7, 30622−30631

formation of Au−Ag bimetallic nanocrystals, the reduced Au^{3+} ions on the AgNC template or the reaction solution were affected by the concentration of the reducing agent.[42] The irradiation light can provide additional energy for accelerating the reduction reaction of Au^{3+} ion in the reaction solution, and this reaction acceleration phenomenon can be observed by the color change of the reaction solution during the reaction. For higher-frequency (higher energy, such as in the HQ mode) irradiation light, the color of the reaction solution changed from colorless to pink. The pink color was due to the reduction of Au^{3+} ions into small Au nanocrystals in the reaction solution, as shown in the TEM image in Supporting Information Figure S3.

However, when a plasmon-induced electromagnetic field was generated using a lower irradiation frequency (such as HD mode), the reduction reaction of Au^{3+} ions in the reaction solution cannot be observed regardless of the irradiation intensity (the number of photons used for photochemical reactions increases with increasing irradiation intensity). This may have resulted from the fact that the irradiation energy was lower than the energy barrier for the reduction of Au^{3+} ions in the solution. To confirm the effect of the irradiation energy on the reduction reaction of Au^{3+} ions in solution, bicomponent nanocrystals were fabricated by galvanic replacement at the frequency of the HQ mode and different irradiation light intensities. Under the conditions of low irradiation light intensity in the HQ mode and low reducing agent concentration (low reducing ability) in the reaction solution, Au^{3+} ions preferentially reduced on the surface of AgNC, thereby generating convex-corner half-cage nanocrystals, as shown in Figure 5A. The reducing ability of Au^{3+} ions in the reaction solution can be enhanced by increasing the intensity of irradiation light, resulting in the formation of a mixed structure of convex-corner half-cage and flowerlike nanocrystals, as shown in Figure 5B. Higher irradiation intensity led to the formation of nanocrystals similar to the flowerlike nanocrystals, as shown in Figure 5C, which was caused by the enhanced reduction reaction in the reaction solution. The phenomenon of enhancing the reducing ability of Au^{3+} ions in the reaction solution can be achieved not only by increasing the intensity of irradiation light but also by increasing the concentration of the reducing agent.[42] Also, the enhanced reducing ability of Au^{3+} ions in the reaction solution also led to the formation of flowerlike nanocrystals in a shorter reaction time, as shown by time-dependent plasmonic spectra in Supporting Information Figure S1.

Potential applications of flowerlike and half-cage-like Au−Ag nanocrystals include serving as excellent catalysts, such as in the reduction of 4-nitrophenol, due to the high surface area/volume ratio of flowerlike nanocrystals and the strong "synergistic effect" of half-cage-like nanocrystals. Also, due to the electron transfer between the semiconductor (Ag_2S) and metal (Ag), Ag_2S-Ag nanocrystals should be used to enhance the catalytic performance. This new synthesis method integrated seed-mediated and plasmon-mediated methods to construct highly nonuniform reaction environments that can be used to synthesize various multicomponent nanocrystals, such as bimetallic or metal−semiconductor nanocrystals. These results suggested that reaction conditions, such as reducing agent concentration, precursor concentration (adjusting the reaction mechanisms), and irradiation wavelength/intensity (adjusting the plasmon-induced "photochemistry"), played important roles in controlling the composition and morphology of nanocrystals. These multicomponent nanocrystals should have multiple functions, benefiting from the inherent properties of each component in the nanocrystal, the "synergistic effect" between different components, and the highly heterogeneous morphology of the nanocrystal, resulting in the high-performance catalysts or chemical sensors.

3. CONCLUSIONS

Here, we demonstrated that highly anisotropic bicomponent nanocrystals can be fabricated by combining seed-mediated and plasmon-induced photochemistry synthesis methods. The highly anisotropic nanocrystals were caused by the highly nonuniform reaction environment around the template nanocrystals. The reaction environment around the template nanocrystals can be controlled by changing the intrinsic environment of the nanocrystals (the plasmon-induced electromagnetic field around them) or the extrinsic environment around the nanocrystals (the area where the template nanocrystals were exposed to the reaction solution). A plasmon-induced electromagnetic field can be tuned by manipulating the intensity and frequency of the irradiation. Also, the exposure area of the nanocrystals in the reaction solution can be controlled by manipulating the position of template nanocrystals in the heterogeneous layer. This new synthesis method is expected to be used to synthesize various multicomponent nanocrystals with well-manipulated morphologies and compositions to produce desired functionalities. These nanocrystals with desirable functions had potential applications, such as photocatalysts, chemical /biosensors, and biomedicine, etc.

4. EXPERIMENTAL SECTION

4.1. Materials. Silver nitrate (≥99%, Fluka), 1,5-pentanediol (98%, ACROS), poly(vinylpyrrolidone) (PVP, M_w = 55,000 (g/mol), Sigma), copper(II) chloride (99%, Sigma), polystyrene (PS, M_w = 35,000 (g/mol), Sigma), hydrogen tetrachloroaurate(III) trihydrate (99.99%, Alfa Aesar), sulfur powder (99.5%, ACROS), sodium sulfide nonahydrate ($Na_2S.9H_2O$, 98%, ACROS), ethanol (95%), toluene (>99.5%, J.T. Baker), and chloroform (99.8%, Macron) were used.

4.2. Synthesis of Shaped AgNCs. AgNCs were synthesized by a previously reported polyol reaction.[46] The $AgNO_3$ precursor solution was prepared by dissolving 0.20 g of $AgNO_3$ and 44 μL of 0.043 M $CuCl_2$ solution in 5 mL of 1,5-pentanediol. The other precursor solution was prepared by dissolving 0.10 g of PVP in 5 mL of 1,5-pentanediol. The reaction solution was prepared by heating 10 mL of 1,5-pentanediol in a 50 mL glass round-bottomed flask under continuous stirring in an oil bath heated to 193 °C. The $AgNO_3$ and PVP precursor solutions were alternately injected into hot 1,5-pentanediol with rates of 500 μL/min and 320 μL/30 s, respectively. The size of AgNC can be controlled by the total volume of precursor injection in the reaction batch. To fabricate the high-uniform heterogeneous nanocrystals, the quality (shape and size) of AgNCs needs to be enhanced, which can be achieved by postsynthetic purification using filter paper. The as-made AgNC colloidal solution possesses ∼20% other shape impurities, such as triangular, spherical, and wirelike nanocrystals, after postsynthetic filtration with a 450 nM filter paper four times and a 220 nM filter paper six times, with the high-uniformity AgNC increasing to >95%.

https://doi.org/10.1021/acsomega.2c04349
ACS Omega 2022, 7, 30622−30631

4.3. Deposition of Polystyrene Thin Films on the Substrate. Silicon/glass substrates were cleaned in a freshly prepared piranha solution (70% (v) concentrated H_2SO_4 and 30% (v) H_2O_2). The substrates were then treated with hexamethyldisilazane (HMDS) vapor to obtain hydrophobic surfaces for enhancing the adhesion force between the substrate and the polymer thin film. PS (M_w = 35,000) was dissolved in a toluene solution (5.8 wt %) for deposition of thin films on the HMDS−Si or HMDS−glass substrate via the spin-coating process. The thickness of polymer films can be controlled by the concentration of the polymer solution and spin speed.

4.4. Deposition of AgNC Arrays on PS Films. To prepare the AgNC array on PS film, the postsynthetic purified AgNC colloidal solution was precipitated in ethanol and then dispersed in $CHCl_3$ for enhancing the evaporation rate during the formation of uniform arrays at the water−air interface by the LB technique. The colloidal solution of AgNCs was then added dropwise to the water−air interface of the glass Petri dish, leaving an isotopically distributed monolayer of silver nanocrystals floating at the water−air interface. The surface tension of the AgNC monolayer array at the water−air interface can be utilized to control the concentration (surface coverage) of the AgNC array. The AgNC monolayer array was then transferred onto the PS films by dip coating. The AgNC array on the PS thin film was embedded into the PS film by thermal treatment at a temperature higher than the glass-transition temperature of PS ($T > T_{g\ of\ PS}$). Also, the embedding depth of AgNCs in PS film can be controlled by thermal treatment conditions (treatment temperature and time).

4.5. Using AgNC Embedding Depth (H) ∼2L/3 in the Polymer Matrix as a Template to Synthesize Au−Ag Bimetallic Nanocrystals under Light Irradiation. A uniform AgNC array was placed in PS (∼200 nm in thickness)—on silicon or glass substrate. Then, AgNC was embedded into PS film with embedding depth H∼L/3 by thermal treatment.[42] This AgNC−PS−glass or silicon substrate was hung in an aqueous solution (as schematically shown in Supporting Information Scheme S1) with light irradiation in HQ and HD modes of the nanocomposite. The 1 mM $HAuCl_4$ solution as the Au^{3+} ion precursor with a specific volume was injected into the reaction solution for the formation of the Au−Ag bimetallic nanocrystals by reducing Au^{3+} ions. Due to the different frequency of irradiation (LED point light source with a power of 9.95 W) at the same reaction condition, such as the Au^{3+} ion concentration condition and PVP concentration, the morphology of bimetallic nanocrystals can be manipulated by the mechanisms of reducing the Au^{3+} ions and plasmon-induced electromagnetic field around nanocrystals. There are several different morphologies of bimetallic nanocrystals: petals on the edges/cores of flowerlike, flowerlike, bumper-corner half-cage, and half-cage-like nanocrystals.

(a) Flowerlike nanocrystals: 8 mg of PVP was dissolved in 12 mL of DI water (0.012 mM) in a 20 mL glass vial. Then, AgNC−PS−glass and Ag−PS−silicon substrates were mounted and hung in a PVP aqueous solution with magnetic stirring (setup schematically shown in Supporting Information Scheme S1) under irradiation in the HD mode and without irradiation. Then, 1.12 mL of 1 mM $AuCl_4^-$ solution was injected every 20 min. The time-dependent optical properties can be characterized by measurement of the extinction spectrum of the AgNC−PS−glass substrate. Also, time-dependent evolution of Au−Ag alloy nanocrystals can be observed by SEM and high-resolution TEM (HRTEM).

(b) Petals on the edges/cores of flowerlike nanocrystals: 8 mg of PVP was dissolved in 12 mL of DI water (0.0012 mM) in a 20 mL glass vial. Then, AgNC−PS−glass and Ag−PS−silicon substrates were mounted and hung in the PVP aqueous solution with magnetic stirring (setup schematically shown in Supporting Information Scheme S1) under irradiation in the HD mode. Then, 1.12 mL of 1 mM $AuCl_4^-$ solution was injected every 20 min. The time-dependent optical properties can be characterized by measurement of the extinction spectrum of the AgNC−PS−glass substrate. Also, time-dependent evolution of Au−Ag alloy nanocrystals can be observed by SEM and HRTEM.

(c) Half-cage-like nanocrystals: 1 mg of PVP was dissolved in 12 mL of DI water (0.0015 mM) in a 20 mL glass vial. Then, AgNC−PS−glass and Ag−PS−silicon substrates were mounted and hung in the PVP aqueous solution with magnetic stirring (setup schematically shown in Supporting Information Scheme S1) under irradiation in the HD mode and without irradiation. Then, 1.12 mL of 1 mM $AuCl_4^-$ solution was injected every 20 min. The time-dependent optical properties can be characterized by measurement of the extinction spectrum of the AgNC−PS−glass substrate. Also, time-dependent evolution of Au−Ag alloy nanocrystals can be observed by SEM and HRTEM.

(d) Bumper-corner half-cage-like nanocrystals: 1 mg of PVP was dissolved in 12 mL of DI water (0.0015 mM) in a 20 mL glass vial. Then, AgNC−PS−glass and Ag−PS−silicon substrates were mounted and hung in the PVP aqueous solution with magnetic stirring under irradiation in the HQ mode. Then, 1.12 mL of 1 mM $AuCl_4^-$ solution was injected every 20 min. The time-dependent optical properties can be characterized by measurement of the extinction spectrum of the AgNC−PS−glass substrate. Also, time-dependent evolution of Au−Ag alloy nanocrystals can be observed by SEM and HRTEM.

The bicomponent nanocrystals in the PS matrix can be removed from the substrate by soaking the substrate in $CHCl_3$. Also, the nanocrystal/PS solution was precipitated by centrifugation to remove PS. The precipitate was redispersed in ethanol for subsequent applications.

4.6. Using AgNC Embedding Depth (H) ∼2L/3 in the Polymer Matrix as a Template to Synthesize Ag_2S-Ag Bicomponent Nanocrystals under Light Irradiation. A uniform AgNC array was placed in PS (∼200 nm in thickness)—on silicon or glass substrate. Then, AgNC was embedded into the PS film with embedding depth H∼L/3 by thermal treatment (as Supporting Information S1) This AgNC−PS−glass or silicon substrate was hung in an aqueous solution (as schematically shown in Supporting Information Scheme S1) with various PVP solutions (stabilizer). The 0.0004 mM Na_2S_x aqueous solution as the S^{2-} ion precursor with a specific volume was injected into the reaction solution for the formation of the Ag_2S-Ag nanocrystals by a sulfidation reaction. Na_2S_x was prepared by dissolving 16.4 mg of sulfur powder and 72.2 mg of Na_2S-$9H_2O$ in 6.3 mL of H_2O (0.047

https://doi.org/10.1021/acsomega.2c04349
ACS Omega 2022, 7, 30622−30631

mM) at 80 °C 12 h. The color of the Na_2S_x aqueous solution was bright yellow. Also, the Na_2S_x aqueous solution was diluted to 0.0004 mM (10 μL of 0.047 mM Na_2S_x aqueous solution + 1.2 mL of H_2O). Due to the different frequency of irradiation (LED point light source with a power of 9.95 W) at the same reaction condition, such as the S^{2-} ion concentration condition and PVP concentration, the morphology of Ag_2S-Ag nanocrystals can be manipulated by the plasmon-induced electromagnetic field around nanocrystals. There are two different morphologies of semiconductor−metal nanocrystals: flowerlike and mushroom-like nanocrystals.

(a) Mushroom-like nanocrystals: 12 mg of PVP was dissolved in 18 mL of DI water (0.018 mM) in a 20 mL glass vial. Then, AgNC−PS−glass and Ag−PS−silicon substrates were mounted and hung in the PVP aqueous solution with magnetic stirring (setup schematically shown in Supporting Information Scheme S1) under irradiation in the HD mode and without irradiation. Then, 10 μL of 0.0004 mM Na_2S_x aqueous solution was injected every 20 min. The time-dependent optical properties can be characterized by measurement of the extinction spectrum of the AgNC−PS−glass substrate. Also, time-dependent evolution of Ag_2S-Ag alloy nanocrystals can be observed by SEM and HRTEM.

(b) Flowerlike nanocrystals: 12 mg of PVP was dissolved in 18 mL of DI water (0.018 mM) in a 20 mL glass vial. Then, AgNC−PS−glass and Ag−PS−silicon substrates were mounted and hung in the PVP aqueous solution with magnetic stirring (setup schematically shown in Supporting Information Scheme S1) under irradiation in the HQ mode. Then, 10 μL of 0.0004 mM Na_2S_x aqueous solution was injected every 20 min. The time-dependent optical properties can be characterized by measurement of the extinction spectrum of the AgNC−PS−glass substrate. Also, time-dependent evolution of Ag_2S-Ag alloy nanocrystals can be observed by SEM and HRTEM.

The bicomponent nanocrystals in the PS matrix can be removed from the substrate by soaking the substrate in $CHCl_3$. Also, the nanocrystal/PS solution was precipitated by centrifugation to remove PS. The precipitate was redispersed in ethanol for subsequent applications.

■ ASSOCIATED CONTENT

Supporting Information

The Supporting Information is available free of charge at https://pubs.acs.org/doi/10.1021/acsomega.2c04349.

Time-dependent optical properties of bicomponent nanocrystals, HRTEM image and EDS spectrum of Ag_2S-Ag nanocrystals, solution color change in different reaction conditions, and scheme of reaction equipment setup (PDF)

■ AUTHOR INFORMATION

Corresponding Author

Su-Wen Hsu − *Department of Chemical Engineering, Nation Cheng Kung University, Tainan City 70101, Taiwan (R.O.C);* orcid.org/0000-0001-6553-3201; Email: swhsu@gs.ncku.edu.tw

Authors

Hsien-Tai Cheng − *Department of Chemical Engineering, Nation Cheng Kung University, Tainan City 70101, Taiwan (R.O.C)*

Ming-Shiuan Huang − *Department of Chemical Engineering, Nation Cheng Kung University, Tainan City 70101, Taiwan (R.O.C)*

Complete contact information is available at: https://pubs.acs.org/10.1021/acsomega.2c04349

Author Contributions

‡H.-T.C. and M.-S.H. contributed equally to this work. S.-W.H. conceived the idea. H.-T.C., M.-S.H., and S.-W.H. designed the research. H.-T.C. and M.-S.H. analyzed the data. The manuscript was written and approved by all authors.

Notes

The authors declare no competing financial interest.

■ ACKNOWLEDGMENTS

This work was supported by a grant from the Ministry of Science and Technology in Taiwan (Contract Nos. MOST 109-2628-E-006-013-MY3 and MOST 108-2218-E-006-056-MY3). The research was also supported in part by Higher Education Sprout Project, Ministry of Education to the Headquarters of University Advancement at National Cheng Kung University (NCKU). The authors acknowledge the NCKU Chemical Engineering facility for use of their scanning electron microscope.

■ REFERENCES

(1) Deng, S. K.; Zhang, B. W.; Choo, P.; Smeets, P. J. M.; Odom, T. W. Plasmonic Photoelectrocatalysis in Copper-Platinum Core-Shell Nanoparticle Lattices. *Nano Lett.* **2021**, *21*, 1523−1529.

(2) Li, L. J.; Jin, J.; Liu, J. J.; Yang, J.; Song, W.; Yang, B.; Zhao, B. Accurate SERS monitoring of the plasmon mediated UV/visible/NIR photocatalytic and photothermal catalytic process involving Ag@ carbon dots. *Nanoscale* **2021**, *13*, 1006−1015.

(3) Lu, C. H.; Li, X. R.; Wu, Q.; Li, J.; Wen, L.; Dai, Y.; Huang, B. B.; Li, B. J.; Lou, Z. Z. Constructing Surface Plasmon Resonance on Bi2WO6 to Boost High-Selective CO2 Reduction for Methane. *ACS Nano* **2021**, *15*, 3529−3539.

(4) Zeng, B.; Wang, S. Y.; Gao, Y. Y.; Li, G. N.; Tian, W. M.; Meeprasert, J.; Li, H.; Xie, H. C.; Fan, F. T.; Li, R. G.; Li, C. Interfacial Modulation with Aluminum Oxide for Efficient Plasmon-Induced Water Oxidation. *Adv. Funct. Mater.* **2021**, *31*, No. 2005688.

(5) Zhang, C. Y.; Jia, F. C.; Li, Z. Y.; Huang, X.; Lu, G. Plasmon-generated hot holes for chemical reactions. *Nano Res.* **2020**, *13*, 3183−3197.

(6) Li, W.; Miao, J. J.; Peng, T. H.; Lv, H.; Wang, J. G.; Li, K.; Zhu, Y.; Li, D. Single-Molecular Catalysis Identifying Activation Energy of the Intermediate Product and Rate-Limiting Step in Plasmonic Photocatalysis. *Nano Lett.* **2020**, *20*, 2507−2513.

(7) Wang, X. X.; Wang, J. G.; Sun, M. T. Plasmon-driven molecular photodissociations. *Appl. Mater. Today* **2019**, *15*, 212−235.

(8) Koopman, W.; Sarhan, R. M.; Stete, F.; Schmitt, C. N. Z.; Bargheer, M. Decoding the kinetic limitations of plasmon catalysis: the case of 4-nitrothiophenol dimerization. *Nanoscale* **2020**, *12*, 24411−24418.

(9) Yang, Q. H.; Xu, Q.; Yu, S. H.; Jiang, H. L. Pd Nanocubes@ZIF-8: Integration of Plasmon-Driven Photothermal Conversion with a Metal-Organic Framework for Efficient and Selective Catalysis. *Angew. Chem., Int. Ed.* **2016**, *55*, 3685−3689.

(10) Wang, W. L.; Zhang, W.; Zhang, D.; Wang, G. P. A low-cost, high-efficiency light absorption structure inspired by the Papilio ulysses butterfly. *RSC Adv.* **2017**, *7*, 22749−22756.

(11) Zhang, Y. C.; He, S.; Guo, W. X.; Hu, Y.; Huang, J. W.; Mulcahy, J. R.; Wei, W. D. Surface-Plasmon-Driven Hot Electron Photochemistry. *Chem. Rev.* **2018**, *118*, 2927−2954.
(12) Vadai, M.; Angell, D. K.; Hayee, F.; Sytwu, K.; Dionne, J. A. In-situ observation of plasmon-controlled photocatalytic dehydrogenation of individual palladium nanoparticles. *Nat. Commun.* **2018**, *9*, No. 4658.
(13) Shi, F. L.; He, J.; Zhang, B. Y.; Peng, J. H.; Ma, Y. L.; Chen, W. L.; Li, F.; Qin, Y.; Liu, Y.; Shang, W.; Tao, P.; Song, C. Y.; Deng, T.; Qian, X. F.; Ye, J.; Wu, J. B. Plasmonic-Enhanced Oxygen Reduction Reaction of Silver/Graphene Electrocatalysts. *Nano Lett.* **2019**, *19*, 1371−1378.
(14) Thomann, I.; Pinaud, B. A.; Chen, Z. B.; Clemens, B. M.; Jaramillo, T. F.; Brongersma, M. L. Plasmon Enhanced Solar-to-Fuel Energy Conversion. *Nano Lett.* **2011**, *11*, 3440−3446.
(15) Li, Z. Y.; Wang, G. L.; Zhang, C. Y.; Wei, C.; Wang, X.; Gao, Y. Q.; Li, H.; Huang, X.; Yuan, H. F.; Lu, G. Silver Nanowire-Templated Molecular Nanopatterning and Nanoparticle Assembly for Surface-Enhanced Raman Scattering. *Chem. - Eur. J.* **2019**, *25*, 10561−10565.
(16) Singh, J.; Dhaliwal, A. S. Plasmon-induced photocatalytic degradation of methylene blue dye using biosynthesized silver nanoparticles as photocatalyst. *Environ. Technol.* **2020**, *41*, 1520−1534.
(17) Atta, A. M.; Moustafa, Y. M.; Al-Lohedan, H. A.; Ezzat, A. O.; Hashem, A. I. Methylene Blue Catalytic Degradation Using Silver and Magnetite Nanoparticles Functionalized with a Poly(ionic liquid) Based on Quaternized Dialkylethanolamine with 2-Acrylamido-2-methylpropane Sulfonate-co-Vinylpyrrolidone. *ACS Omega* **2020**, *5*, 2829−2842.
(18) Wan, G. P.; Peng, X. E.; Zeng, M.; Yu, L.; Wang, K.; Li, X. Y.; Wang, G. Z. The Preparation of Au@TiO2 Yolk-Shell Nanostructure and its Applications for Degradation and Detection of Methylene Blue. *Nanoscale Res. Lett.* **2017**, *12*, No. 535.
(19) Halas, N. J.; Lal, S.; Chang, W. S.; Link, S.; Nordlander, P. Plasmons in Strongly Coupled Metallic Nanostructures. *Chem. Rev.* **2011**, *111*, 3913−3961.
(20) Hartland, G. V. Optical Studies of Dynamics in Noble Metal Nanostructures. *Chem. Rev.* **2011**, *111*, 3858−3887.
(21) Lang, X. J.; Chen, X. D.; Zhao, J. C. Heterogeneous visible light photocatalysis for selective organic transformations. *Chem. Soc. Rev.* **2014**, *43*, 473−486.
(22) Liang, C.; Lu, Z. A.; Wu, J.; Chen, M. X.; Zhang, Y. Y.; Zhang, B.; Gao, G. L.; Li, S. W.; Xu, P. Recent Advances in Plasmon-Promoted Organic Transformations Using Silver-Based Catalysts. *ACS Appl. Mater. Interfaces.* **2020**, *12*, 54266−54284.
(23) Wang, M. Y.; Ye, M. D.; Iocozzia, J.; Lin, C. J.; Lin, Z. Q. Plasmon-Mediated Solar Energy Conversion via Photocatalysis in Noble Metal/Semiconductor Composites. *Adv. Sci.* **2016**, *3*, No. 1600024.
(24) Ueno, K.; Oshikiri, T.; Sun, Q.; Shi, X.; Misawa, H. Solid-State Plasmonic Solar Cells. *Chem. Rev.* **2018**, *118*, 2955−2993.
(25) Wang, C. L.; Astruc, D. Nanogold plasmonic photocatalysis for organic synthesis and clean energy conversion. *Chem. Soc. Rev.* **2014**, *43*, 7188−7216.
(26) Long, R.; Li, Y.; Song, L.; Xiong, Y. J. Coupling Solar Energy into Reactions: Materials Design for Surface Plasmon-Mediated Catalysis. *Small* **2015**, *11*, 3873−3889.
(27) Linic, S.; Christopher, P.; Ingram, D. B. Plasmonic-metal nanostructures for efficient conversion of solar to chemical energy. *Nat. Mater.* **2011**, *10*, 911−921.
(28) Christopher, P.; Xin, H. L.; Linic, S. Visible-light-enhanced catalytic oxidation reactions on plasmonic silver nanostructures. *Nat. Chem.* **2011**, *3*, 467−472.
(29) Brongersma, M. L.; Halas, N. J.; Nordlander, P. Plasmon-induced hot carrier science and technology. *Nat. Nanotechnol.* **2015**, *10*, 25−34.
(30) Heo, M.; Cho, H.; Jung, J. W.; Jeong, J. R.; Park, S.; Kim, J. Y. High-Performance Organic Optoelectronic Devices Enhanced by Surface Plasmon Resonance. *Adv. Mater.* **2011**, *23*, 5689.
(31) Zhang, J. J.; Xiao, S. S.; Wubs, M.; Mortensen, N. A. Surface Plasmon Wave Adapter Designed with Transformation Optics. *ACS Nano* **2011**, *5*, 4359−4364.
(32) Buddhiraju, S.; Shi, Y.; Song, A.; Wojcik, C.; Minkov, M.; Williamson, I. A. D.; Dutt, A.; Fan, S. H. Absence of unidirectionally propagating surface plasmon-polaritons at nonreciprocal metal-dielectric interfaces. *Nat. Commun.* **2020**, *11*, No. 674.
(33) Yu, R. W.; Liz-Marzan, L. M.; de Abajo, F. J. G. Universal analytical modeling of plasmonic nanoparticles. *Chem. Soc. Rev.* **2017**, *46*, 6710−6724.
(34) Sun, M. H.; Li, Y.; Zhang, B.; Argyropoulos, C.; Sutter, P.; Sutter, E. Plasmonic Effects on the Growth of Ag Nanocrystals in Solution. *Langmuir* **2020**, *36*, 2044−2051.
(35) Zhao, W. J.; Zhang, W. X.; Wang, R. Y.; Ji, Y. L.; Wu, X. C.; Zhang, X. D. Photocontrollable Chiral Switching and Selection in Self-Assembled Plasmonic Nanostructure. *Adv. Funct. Mater.* **2019**, *29*, No. 1900587.
(36) Lan, X.; Zhou, X.; McCarthy, L. A.; Govorov, A. O.; Liu, Y.; Link, S. DNA-Enabled Chiral Gold Nanoparticle-Chromophore Hybrid Structure with Resonant Plasmon-Exciton Coupling Gives Unusual and Strong Circular Dichroism. *J. Am. Chem. Soc.* **2019**, *141*, 19336−19341.
(37) Guo, W. X.; Johnston-Peck, A. C.; Zhang, Y. C.; Hu, Y.; Huang, J. W.; Wei, W. D. Cooperation of Hot Holes and Surface Adsorbates in Plasmon-Driven Anisotropic Growth of Gold Nanostars. *J. Am. Chem. Soc.* **2020**, *142*, 10921−10925.
(38) Zhai, Y. M.; DuChene, J. S.; Wang, Y. C.; Qiu, J. J.; Johnston-Peck, A. C.; You, B.; Guo, W. X.; DiCiaccio, B.; Qian, K.; Zhao, E. W.; Ooi, F.; Hu, D. H.; Su, D.; Stach, E. A.; Zhu, Z. H.; Wei, W. D. Polyvinylpyrrolidone-induced anisotropic growth of gold nanoprisms in plasmon-driven synthesis. *Nat. Mater.* **2016**, *15*, 889.
(39) Golze, S. D.; Hughes, R. A.; Rouvimov, S.; Neal, R. D.; Demille, T. B.; Neretina, S. Plasmon-Mediated Synthesis of Periodic Arrays of Gold Nanoplates Using Substrate-Immobilized Seeds Lined with Planar Defects. *Nano Lett.* **2019**, *19*, 5653−5660.
(40) Wu, X. M.; Thrall, E. S.; Liu, H. T.; Steigerwald, M.; Brus, L. Plasmon Induced Photovoltage and Charge Separation in Citrate-Stabilized Gold Nanoparticles. *J. Phys. Chem. C* **2010**, *114*, 12896−12899.
(41) Sutter, P.; Li, Y.; Argyropoulos, C.; Sutter, E. In Situ Electron Microscopy of Plasmon-Mediated Nanocrystal Synthesis. *J. Am. Chem. Soc.* **2017**, *139*, 6771−6776.
(42) Jhang, W. L.; Huang, M. S.; Hsu, S. W. Unsymmetrical Heterogeneous Au-Ag Nanocrystals as Catalysts, Sensors, and Drug Carriers. *ACS Appl. Nano Mater.* **2021**, *4*, 10011−10017.
(43) Zhang, S. P.; Bao, K.; Halas, N. J.; Xu, H. X.; Nordlander, P. Substrate-Induced Fano Resonances of a Plasmonic: Nanocube: A Route to Increased-Sensitivity Localized Surface Plasmon Resonance Sensors Revealed. *Nano Lett.* **2011**, *11*, 1657−1663.
(44) Collins, G.; McCarty, E. K.; Holmes, J. D. Controlling alloy formation and optical properties by galvanic replacement of sub-20 nm silver nanoparticles in organic media. *Crystengcomm* **2015**, *17*, 6999−7005.
(45) Yadav, V.; Jeong, S.; Ye, X. C.; Li, C. W. Surface-Limited Galvanic Replacement Reactions of Pd, Pt, and Au onto Ag Core Nanoparticles through Redox Potential Tuning. *Chem. Mater.* **2022**, *34*, 1897−1904.
(46) Tao, A. R.; Habas, S.; Yang, P. D. Shape control of colloidal metal nanocrystals. *Small* **2008**, *4*, 310−325.

https://doi.org/10.1021/acsomega.2c04349
ACS Omega 2022, 7, 30622−30631